Effect of Alkyl Silicone Oil on the Compatibility of Polypropylene/Microencapsulated Ammonium Polyphosphate Composites

Zhi-Ling Ma, Guang-Yu Lu

College of Chemistry and Environmental Science, Hebei University, Baoding 071002, China

Received 19 August 2010; accepted 21 October 2010
DOI 10.1002/app.33613
Published online 28 February 2011 in Wiley Online Library (wileyonlinelibrary.com).

ABSTRACT: The effect of alkyl silicone oil (ASO) as a compatibilizer on the compatibility of polypropylene (PP)/microencapsulated ammonium polyphosphate (MAPP) composites was investigated. The data from the mechanical tests showed that when 0.25% ASO was added, the tensile strength of the PP/MAPP/ASO composites increased approximately 41% compared with that of the PP/MAPP composite. The scanning electron microscopy results illustrate that ASO improved the interfacial adhesion between MAPP and PP. Polarized optical microscopy and X-ray diffraction demonstrated that ASO decreased the agglomeration of MAPP and made MAPP disperse homogeneously in PP. Flow tests and IR spectroscopy indicated that ASO played the role of lubricant in PP/MAPP, and the flow behavior of composites in the melt was that of a pseudoplastic liquid, in which MAPP interacted with ASO by molecular interaction. All of the investigations showed that a suitable amount of ASO improved the compatibility of the PP/MAPP composite. © 2011 Wiley Periodicals, Inc. J Appl Polym Sci 121: 1176–1182, 2011

Key words: compatibility; flame retardance; microencapsulation; poly(propylene) (PP); polysiloxanes

INTRODUCTION

Polypropylene (PP) is a widely used but easily burned polymer, and thus, it is necessary to improve its flame retardancy.[1–3] In recent years, intumescent flame retardants (IFR) have attracted more and more attention because they produce low smoke and low toxicity with no corrosive gas generation.[4] It is well known that typical IFR additives are based on an acid source, a char source, and a blowing source, such as the ammonium phosphate/pentaerythritol/melamine system.[5–8] However, these highly polar IFRs face the problems of water leaching and exudation; moreover, the high loadings of IFR additives greatly damage the mechanical properties of PP/IFRs because of the poor compatibility between IFRs and nonpolar PP.[9] To improve the compatibility, compatibilizers, such as carboxylated PP;[10,11] the use of a silane coupling agent (KH-550)[10,12] and silicone oil;[13,14] and so on have been used in PP/IFRs. Wang et al.[13] found that methyl hydrogen siloxane improved the compatibility of PP/IFRs, and Chen and Jiao[14] proved that a suitable amount of hydroxy silicone oil played a synergistic effect on the flame retardancy of PP/IFR composites.

Correspondence to: Z.-L. Ma (zhilingma838838@163.com).

Journal of Applied Polymer Science, Vol. 121, 1176–1182 (2011)

Silicone oil is a macromolecular silicon compound with Si—O—Si bonds as its main-chain groups and methyl as its side chain. It has many good properties, including good water resistance, chemical stability, good lubrication, antifouling properties, antitacking properties, printability, and strong affinity to organic materials. Alkyl silicone oil (ASO) is the product of the partial replacement of the methyl groups in silicone oil with long alkyl chains. Compared with the methyl groups, the long alkyl chains are more compatible with PP, so ASO was chosen as the compatibilizer in this study.

In our previous study,[15] microencapsulated ammonium polyphosphate (MAPP), as a new IFR, was prepared. It had excellent flame retardancy, low water solubility, and no exudation in PP/MAPP. The purpose of this study was to investigate the effects of ASO as a compatibilizer in PP/MAPP composites.

EXPERIMENTAL

Materials

PP (type T30S, density $d = 0.901$ g/cm^3) was supplied by PetroChina Co., Ltd., Daqing Branch (Daqing, China). Ammonium polyphosphate [APP; type FR-II, molecular formula: $(NH_4PO_3)_n$, where $n > 1000$, $P_2O_5 \geq 70$–71%, nitrogen $N \geq 13$–14%] was purchased from Xusen Nonhalogen Smoke Suppressing Fire retardants Co., Ltd. (Shanghai, China). APP

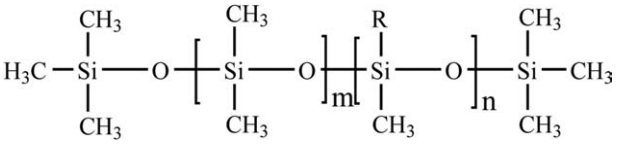

Scheme 1 Chemical structure of ASO.

was microencapsulated by melamine–formaldehyde resin according to ref. 15 (melamine–formaldehyde resin/APP = 1 : 3 w/w), so MAPP ($P_2O_5 \geq 50\%$) was prepared. ASO (type DY-A601), whose chemical structure is shown in Scheme 1, was obtained from Shandong Dayi Chemical Co., Ltd. (Shandong, China).

Equipment and analysis procedures

The tensile strengths were measured with a WSM-20KN test apparatus (Intelligent Instrument and Equipment Co., Ltd., Changchun, China) according to the GB/T 1040-2006 standard. The testing was conducted at room temperature, and the reported data are the averages of five measurements.

The ease of ignition of PP was studied according to the GB/T 2408-1996 horizontal standard, with sheet dimensions of 127 × 12.7 × 3.5 mm^3 and with a Bunsen burner being ignited for 30 s. The combustion time, flame-spread rate, and extinguishing time (ET) were recorded. The limiting oxygen index (LOI) values were measured on a JF-3 oxygen index meter (Nanjing Leiqiong Equipment Co., Ltd., Nanjing, China) according to GB/T 2406-1993, with sheet dimensions of 130 × 6.5 × 3 mm^3.

The morphologies of the tensile fracture surfaces of the samples were observed with a (Beijing Scientific Instruments Company, Chinese Academy of Sciences, Beijing, China). KYKY-2800B scanning electron microscope (KYKY Technology Development, Ltd., Beijing, China) after a gold-coating surface treatment; the electron micrographs were taken at an acceleration voltage of 25.0 kV. The crystal morphologies of the samples were observed with a 59XA polar optical microscope (Shanghai Optic Apparatus Co., Ltd., Shanghai, China) and were magnified 100 times. The crystal structures of the composites were measured by a Y-4Q X-ray diffractometer (Dandong Radiative Instrument Co., Ltd., Dandong, China) with Cu Kα radiation.

The rheological behavior was determined by an XLY-II high-pressure capillary rheometer (Science and Education Instrument Factory of Jilin University, Changchun, China). The diameter and length-to-diameter ratio of the capillary were 1 mm and 20, respectively. The temperature of the instruments was fixed at 180°C, and the experimental loads were 100, 120, 140, 160, and 180 kg/cm^2.

IR spectra were recorded on a TNZ1-Nicolet 380 IR spectroscopy instrument (Thermo Fisher Scientific, USA).

MAPP modified by ASO

The MAPP powder and ASO were kneaded in a ZH-0.5 kneader (Enso Technology Co., Ltd., Nanjing, China) at 130°C for 10 min, and the weight-to-weight ratios of MAPP/ASO were 350/1.75, 350/3.50, 350/5.25, 350/7.00, and 350/8.75 w/w.

Preparation of the PP/MAPP/ASO composites

The ratios of PP/MAPP/ASO were 75/25/0.125, 75/25/0.250, 75/25/0.375, 75/25/0.500, and 75/25/0.625 w/w/w. The composites were prepared at 170–180°C in a two-roll mill (XKR-160 type, Zhanjiang Machinery Factory of Guangdong, Zhanjiang, China). After the PP melted, the modified MAPP was added. Next, the composite was mixed for 10 min and removed for compression molding at 180°C for 3 min; finally, the composite was cooled to room temperature by cool pressing. After being annealed at 70–80°C for 8 h, the specimen was operated on a ZHY-W almighty (Chengde Experimental Factory, Chengde, China) sample preparing machine.

Preparation of the polarized optical microscopy (POM) samples

The compression-molded film sample was sandwiched between two cover glasses and was kept on a hot plate at 200°C for 10 min so it could melt completely. Then, it was transferred to a 200°C oven, cooled naturally to 142°C, isothermally crystallized at 142°C for 3 h, and finally, cooled naturally to room temperature.

Preparation of the X-ray diffraction (XRD) samples

The composites were compression-molded at 180°C for 3 min and were then cooled to room temperature by cool pressing to prepare 1-mm-thick sheets for the XRD collection data.

Preparation of the IR spectroscopy samples

MAPP modified by ASO (MAPP/ASO = 1/1 w/w) was wrapped in a filter paper, extracted with xylene in a Soxhlet apparatus for 72 h for unreacted ASO to be washed off, and finally, dried for IR analysis.

RESULTS AND DISCUSSION

Effect of ASO on the properties of PP/MAPP

In our previous study, PP/MAPP had obvious flame retardancy when the MAPP content exceeded 25%, so a mass fraction of PP/MAPP = 75/25 was chosen.[15]

TABLE I
Effect of ASO on the Properties of the PP/MAPP Composites

Sample	PP/MAPP/ASO (w/w/w)	Tensile strength (MPa)	Horizontal combustion test		LOI (%)
			Rate	Extinguish Time ET	
A	100/0/0	36.1	Burn and dripping	—	17.4
B	75/25/0	23.2	FH-1 and intumescent	2	31.0
C	75/25/0.125	26.9	FH-1 and intumescent	4.7	28.1
D	75/25/0.250	32.6	FH-2 and intumescent	3.3	30.3
E	75/25/0.375	29.4	FH-3 and intumescent	0	31.5
F	75/25/0.500	27.4	FH-4 and intumescent	3.7	29.2
G	75/25/0.625	25.7	FH-5 and intumescent	4.7	27.9

Because of the poor compatibility of PP and MAPP, it was almost impossible to prepare MAPP/PP blends with good mechanical properties. As shown by composite B in Table I, the addition of 25 g of MAPP to 75 g of PP provided good flame retardancy, intumescence, and no dripping, but the mechanical properties decreased drastically. For the compatibility to be improved, MAPP was modified by ASO. As shown in Table I, the mechanical properties of composites C, D, E, F, and G were significantly improved. In particular, when 0.25% ASO was added, the tensile strength of composite D (PP/MAPP/ASO = 75/25/0.25) achieved a maximum value and was enhanced by 41% compared to that of PP/MAPP. All of these results indicate that there was an optimum value of ASO loading for improving the mechanical properties of the PP/MAPP composites. Meanwhile, the flame retardancy of the composites changed negligibly. This demonstrated that the compatibility between the MAPP dispersed phase and the PP matrix phase was improved by ASO.

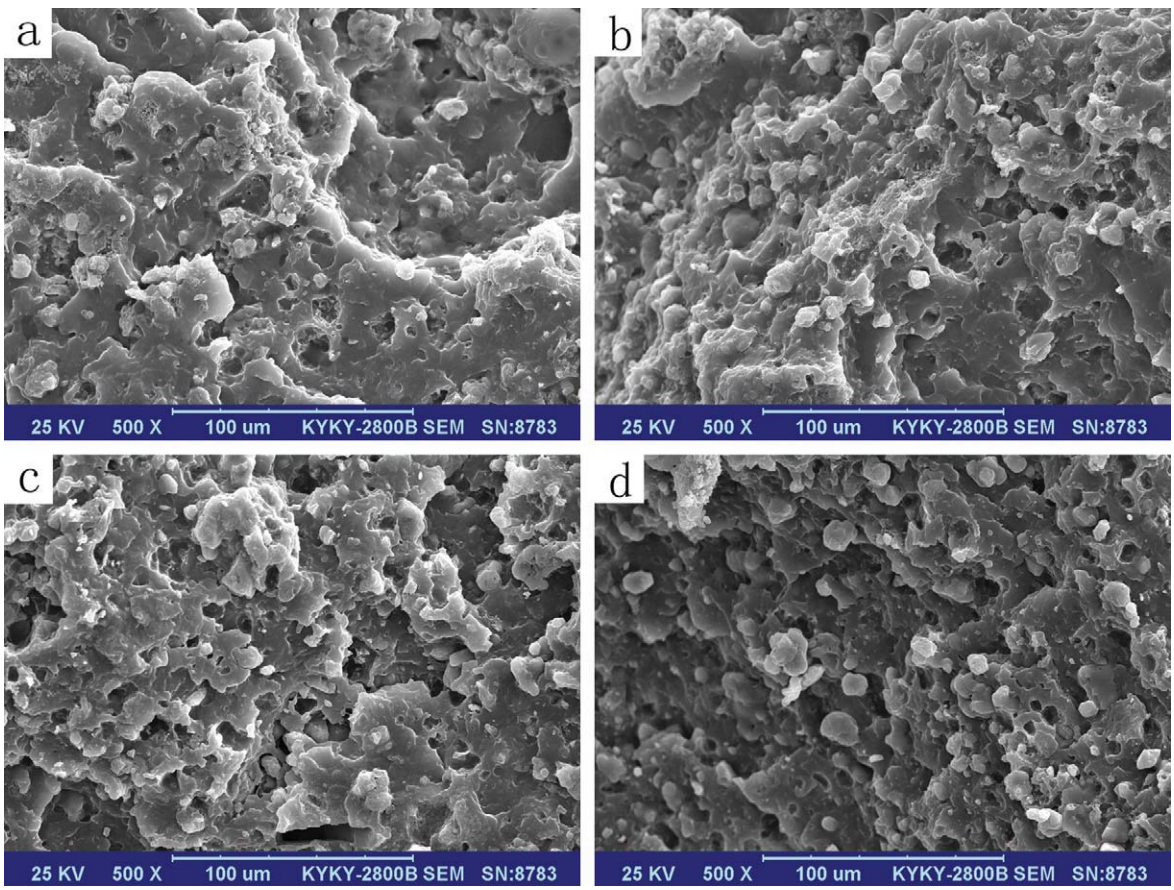

Figure 1 SEM micrographs of the tensile fracture surfaces of the composites. (a) PP/MAPP = 75/25, (b) PP/MAPP/ASO = 75/25/0.125, (c) PP/MAPP/ASO = 75/25/0.250, and (d) PP/MAPP/ASO = 75/25/0.375. [Color figure can be viewed in the online issue, which is available at wileyonlinelibrary.com.]

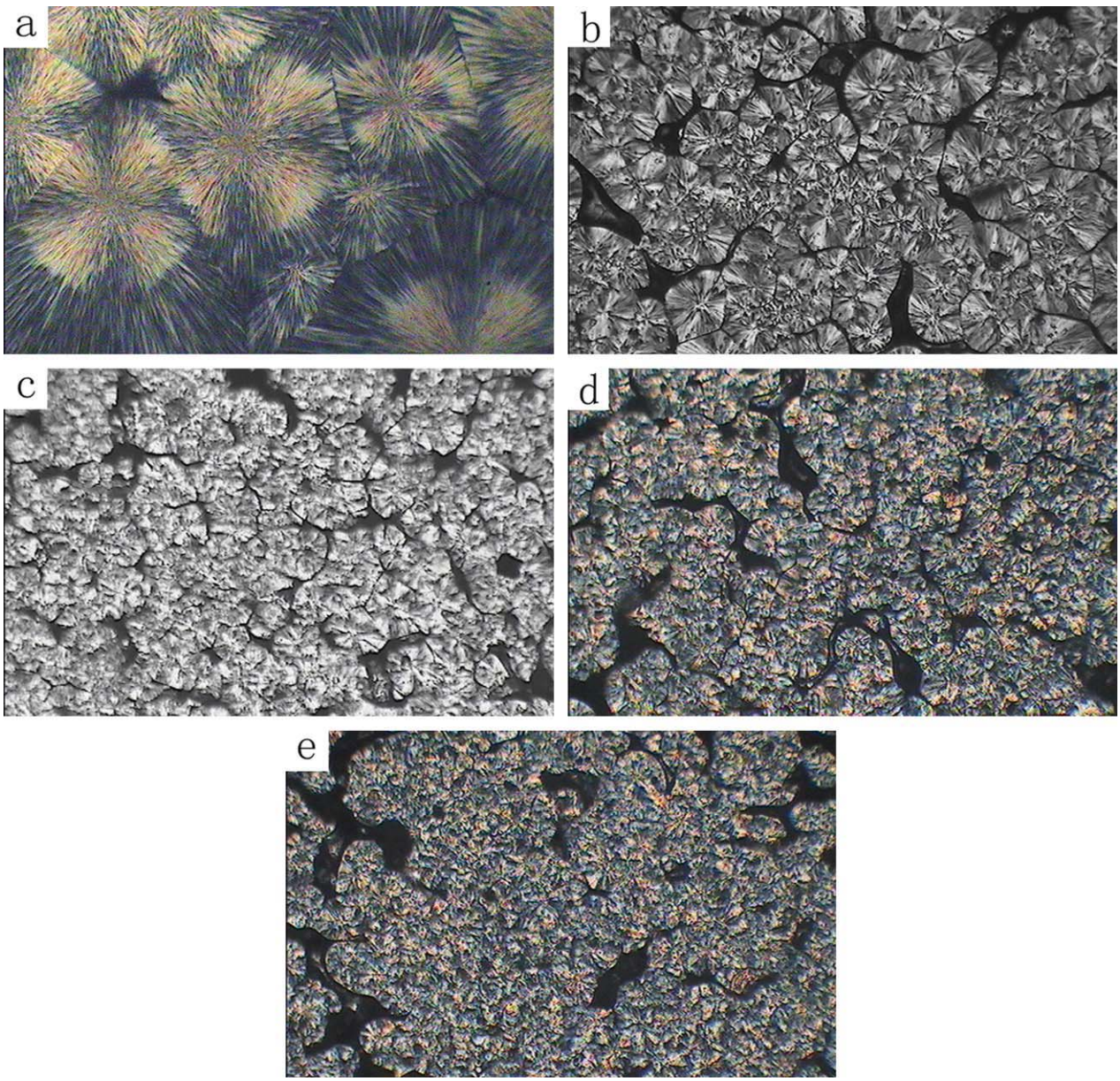

Figure 2 POM micrographs of the crystal of the composites: (a) PP, (b) PP/MAPP = 49/1, (c) PP/MAPP/ASO = 49/1/0.005, (d) PP/MAPP/ASO = 49/1/0.010, and (e) PP/IFR/ASO = 49/1/0.015. [Color figure can be viewed in the online issue, which is available at wileyonlinelibrary.com.]

Morphology

Morphology is an important way to characterize the compatibility of composites directly. Here, we investigated the morphology with scanning electron microscopy (SEM) and POM.

Figure 1 shows the SEM micrographs of the tensile fracture surfaces of the composites. Figure 1(a) (PP/MAPP composite) shows that the interface between MAPP and PP was not clear, and the surface of the remaining holes appeared to be very smooth. This means that the adhesion between MAPP and PP was poor. As ASO was added [Fig. 1(b–d)], MAPP dispersed homogeneously, and the interface of MAPP and the matrix became less well defined; this implies that ASO enhanced the interfacial adhesion of PP/MAPP, improved the dispersability of MAPP in PP, and increased the mechanical properties.

Figure 2 shows the POM micrographs of the composite samples. It was not easy to observe the crystal morphology of PP/MAPP with a high content of MAPP, so low-content MAPP composites were prepared for POM analysis.

In Figure 2(a), we observed perfectly spherical crystals of pure PP and derived spherulites, which impinged upon each other. Figure 2(b) shows that the crystal morphology of PP was greatly affected by the addition of MAPP because the sizes of the

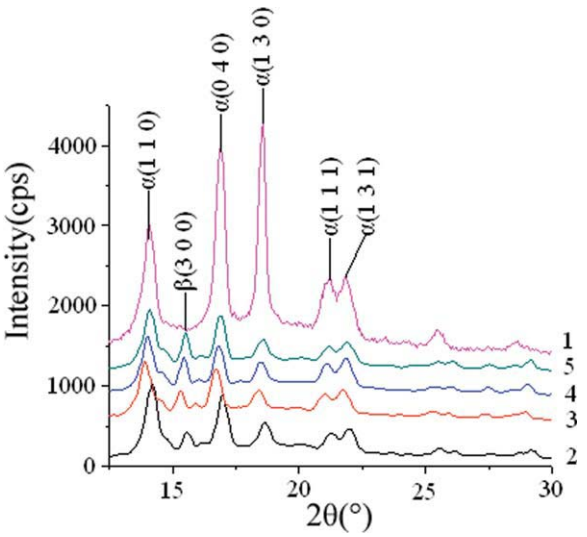

Figure 3 XRD patterns of PP/MAPP/ASO: (1) PP/MAPP/ASO = 100/0/0, (2) PP/MAPP/ASO = 75/25/0, (3) PP/MAPP/ASO = 75/25/0.125, (4) PP/MAPP/ASO = 75/25/0.250, and (5) PP/MAPP/ASO = 75/25/0.375. [Color figure can be viewed in the online issue, which is available at wileyonlinelibrary.com.]

spherulites decreased significantly and they were dispersed nonuniformly. The spherulites were smaller in the places where more MAPP was dispersed and were larger where there was less or no MAPP. The reason might be that the MAPP served as seeds for spherulite growth in PP; this resulted in the growth of crystals on the surface of the MAPP particles.

The crystal morphology of the PP/MAPP/ASO composites can be observed in Figure 2(c–e). Compared with Figure 2(b), these figure parts clearly show that MAPP dispersed into the PP matrix homogeneously, and PP preferably appeared to have crystallized over the MAPP domain surface. With the addition of ASO, the average size of the spherulites became smaller, and their distribution became narrow and uniform. Meanwhile, the interface between the spherulites became more and more blurred; this implies that β crystallinity of PP occurred.[16]

XRD

Figure 3 shows the XRD patterns for PP, PP/MAPP, and PP/MAPP/ASO. As shown in curve 1, pure PP showed five prominent peaks in the 2θ range 10–30°, which corresponded to the monoclinic α-crystalline phase, with the preferential crystallographic orientations (130) and (040). However, the preferential crystallographic orientations were (110) and (040) in the PP/MAPP composite (curve 2), and in addition, a diffraction peak at 2θ = 15.58°, corresponding to the β(300) plane, appeared clearly. Curves 3–5 in Figure 3 correspond to the PP/MAPP/ASO composites with different ASO contents. As shown in Figure 3, as ASO increased, the intensity of β(300) increased.

$$K_\beta = \frac{I_\beta(300)}{I_\alpha(110) + I_\alpha(040) + I_\alpha(130) + I_\alpha(300)}$$

Scheme 2 Calculation formula of K_β.

Table II shows the intensity changes in the main α phases and β crystal further, from which the intensities of the five prominent peaks and the relative content of β crystals (K_β) could be defined by the calculation formula shown in Scheme 2,[16] where $I_\alpha(110)$, $I_\alpha(040)$, $I_\alpha(130)$, and $I_\beta(300)$ correspond to the diffraction peak intensities of the α(110), α(040), α(130), and β(300) planes, respectively. The units are counts per second (cps) of the photons.

In the PP/MAPP composite, K_β increased from 5.7% of pure PP to 16.45%. This indicates that MAPP affected the crystal structure of the PP matrix and promoted β-crystal formation in PP.

In PP/MAPP/ASO, as the ASO concentration increased, K_β increased. The reasons may have been that MAPP had fewer agglomerates and dispersed homogeneously and the adherent points between MAPP and PP were distributed more extensively. The results of XRD agreed very well with that of POM and SEM.

All of the previously discussed results showed that ASO improved the interaction between MAPP and PP.

Rheological behavior of the composites

An XLY-II (Science and Education Instrument Factory of Jilin University, Changchun, China.) flow tester was used to investigate the rheological behavior of

TABLE II
XRD Intensity and K_β Values of the PP/MAPP/ASO Composites

Sample	PP/MAPP/ASO (w/w/w)	$I_\alpha(110)$ (cps)	$I_\alpha(040)$ (cps)	$I_\alpha(130)$ (cps)	$I_\beta(300)$ (cps)	K_β (%)
1	100/0/0	1713	2652	2989	446	5.70
2	75/25/0	1146	954	591	530	16.45
3	75/25/0.125	888	805	473	597	21.61
4	75/25/0.250	922	770	545	790	26.10
5	75/25/0.375	942	878	509	825	26.30

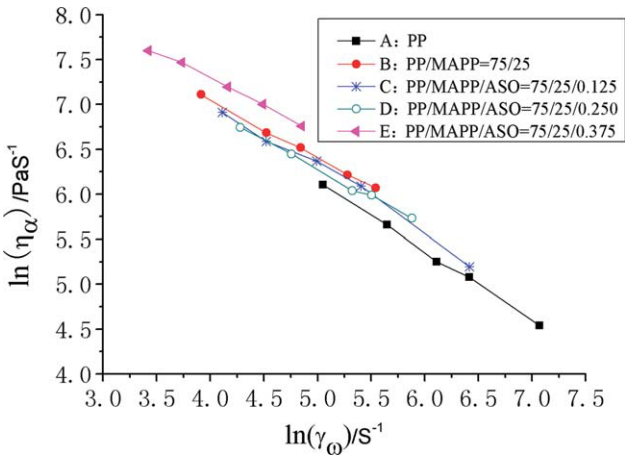

Figure 4 Rheological behavior of the PP/MAPP/ASO composites (180°C). [Color figure can be viewed in the online issue, which is available at wileyonlinelibrary.com.]

the composites. A plot of the apparent viscosity (ln η_α) versus shear rate (ln γ_ω) is shown in Figure 4. Compared with pure PP (line A), the η_α value of the PP/MAPP composite (line B) increased at a given ln γ_ω's because MAPP restricted the PP molecular motion and caused a resistance to flow. With the addition of ASO, the ln η_α values of composites C and D decreased at defined ln γ_ω values; this indicated that ASO played the role of a lubricant or plasticizer. However, when more ASO was added, ln η_α increased in composite E, perhaps because the interface of MAPP and PP might have been replaced by that of ASO and PP. We suggest, therefore, that a suitable amount of ASO reduced ln η_α and made a more homogeneous dispersion of MAPP in the PP system.

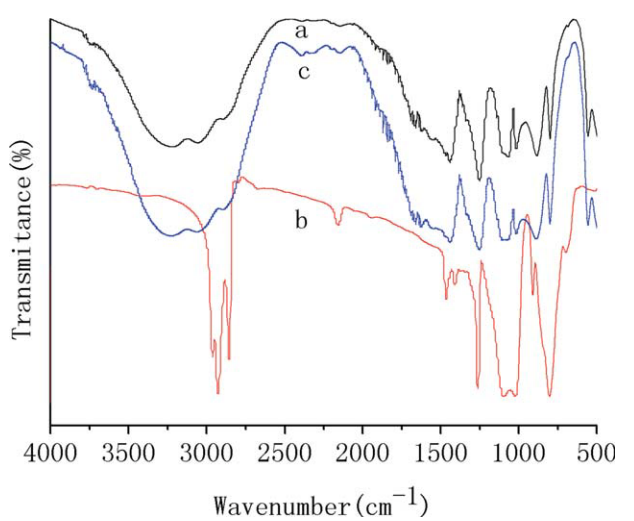

Figure 5 FTIR spectra of (a) MAPP, (b) ASO, and (c) MAPP/ASO. [Color figure can be viewed in the online issue, which is available at wileyonlinelibrary.com.]

In addition, ln η_α of the composites decreased as ln γ_ω increased, and the linear trend implied that the melt was a pseudoplastic liquid and had good processability.

Mechanism of compatibility

Figure 5 shows the FTIR spectra of MAPP, MAPP/ASO, and ASO. In Figure 5(c) is shown the FTIR of MAPP/ASO that was extracted with xylene for 72 h for the unreacted ASO to be washed off. In contrast with Figures 5(a) and 5(b), Figure 5(c) does not show the characteristic peaks of ASO; for example, at 1261.09 cm^{-1}, there is no sharp and strong asymmetrical absorption of the $Si(CH_3)_2$ group of ASO. The results of Figure 5(c) demonstrate that ASO reacted with MAPP. Thus, ASO covered the surfaces of MAPP mainly by quite strong intermolecular action.

CONCLUSIONS

1. The tests of the mechanical properties showed that a defined amount of ASO improved the tensile strength of PP/MAPP without changing the overall flame retardancy.
2. The SEM results indicate that ASO improved the adhesion between MAPP and PP and caused MAPP particles to be better dispersed into the polymer matrix.
3. POM and XRD illustrated that MAPP promoted β-crystal formation in PP. With the addition of ASO, MAPP had fewer agglomerates and dispersed more homogeneously; this resulted in an increase in K_β.
4. IR spectroscopy showed that ASO covered and reacted with the surfaces of MAPP mainly by intermolecular force interactions rather than by the formation of covalent bonds. The rheological behavior indicated that ASO played the role of an internal lubricant or plasticizer.

All of the results indicate that ASO was a true compatibilizer for the PP/MAPP composites and that the addition of a defined amount of ASO had an excellent compatible effect on the PP/MAPP composites.

References

1. Marosfoi, B. B.; Garas, S.; Bodzay, B.; Zubonyai, F.; Marosi, G. Polym Adv Technol 2008, 19, 693.
2. Zhang, M.; Ding, P.; Qu, B. J. Polym Compos 2009, 30, 1000.
3. Jiao, C. M.; Chen, X. L. Polym Eng Sci 2010, 50, 767.
4. Peng, H. Q.; Zhou, Q.; Wang, D. Y.; Chen, L.; Wang, Y. Z. J Ind Eng Chem 2008, 14, 589.
5. Albright, J. A. Br. Pat. 1,517,652 (1976).
6. Camino, G. Polym Degrad Stab 1989, 25, 277.
7. Zhang, P.; Song, L.; Lu, H. D.; Hua, Y.; Xing, W. Y.; Ni, J. X.; Wang, J. Polym Degrad Stab 2009, 94, 201.
8. Wu, K.; Wang, Z. Z.; Liang, H. J. Polym Compos 2008, 29, 854.

9. Vahabodin, G.; Seyed, A. M.; Mahmood, T. A.; Siamak, M. J Appl Polym Sci 2008, 110, 2971.
10. Ma, Z. L.; Guo, H. Y.; Jia, W.; Yang, X. J. J Appl Polym Sci 2007, 106, 411.
11. Ma, Z. L.; Guo, H. Y. J Appl Polym Sci 2007, 104, 66.
12. Ma, Z. L.; Wang, J. H.; Zhang, X. Y. J Appl Polym Sci 2008, 107, 1000.
13. Wang, X. Y.; Li, Y.; Liao, W. W.; Gu, J.; Li, D. Polym Adv Technol 2008, 19, 1060.
14. Chen, X. L.; Jiao, C. M. Fire Safety J 2009, 44, 1010.
15. Ma, Z. L.; Tang, H. P.; Lu, Z. Y.; Wang, Y. F.; Zhai, W. Q. China Plast 2009, 23, 76.
16. Hu, C. X.; Zhang, W. J.; Xue, J. W. J Taiyuan Univ Technol 2006, 37, 618.